Redox dynamics of Ni catalysts in CO_2 reforming of methane

Katharina Mette,[a] Stefanie Kühl,[a] Andrey Tarasov,[a] Hendrik Düdder,[b] Kevin Kähler,[b] Martin Muhler,[b] Robert Schlögl,[a] Malte Behrens*[a]

[a] K. Mette, Dr. S. Kühl, Dr. A. Tarasov, Prof. Dr. R. Schlögl, Dr. M. Behrens

Department of Inorganic Chemistry

Fritz Haber Institute of the Max Planck Society

Faradayweg 4-6, 14195 Berlin (Germany)

Fax: (+49) 30-8413-4405

E-mail: behrens@fhi-berlin.mpg.de

http://www.fhi-berlin.mpg.de/

[b] Hendrik Düdder, Dr. K. Kähler, Prof. Dr. M. Muhler

Ruhr-Universität Bochum

Lehrstuhl für Technische Chemie

Universitätsstraße 150, 44801 Bochum (Germany)

Keywords: Dry Reforming of Methane / Nickel / Coking / Ni,Mg,Al Hydrotalcite / High Temperature / Redox dynamics

Abstract

The influence of redox dynamics of a Ni/MgAl oxide catalyst for dry reforming of methane (DRM) at high temperature was studied to correlate structural stability with catalytic activity and coking propensity. Structural aging of the catalyst was simulated by repeated temperature-programmed reduction / oxidation (TPR/TPO) cycles. Despite a very high Ni loading of 55.4 wt.-%, small Ni nanoparticles of 11 nm were obtained from a hydrotalcite-like precursor with a homogeneous distribution. Redox cycling gradually changed the interaction of the active Ni phase with the oxide support resulting in a crystalline Ni/$MgAl_2O_4$-type catalyst. After cycling the average particle size increased from 11 to 21 nm - while still a large fraction of small particles was present - bringing about a decrease in Ni surface area of 72%. Interestingly, the redox dynamics and its strong structural and chemical consequences were found to have only a moderate influence on the activity in DRM at 900 °C, but lead to a stable attenuation of carbon formation due to a lower fraction of graphitic carbon after DRM in a fixed-bed reactor. Supplementary DRM experiments in a thermobalance revealed that coke formation as a continuous process until a carbon limit is reached and confirmed a higher coking rate for the cycled catalyst.

1 Introduction

Fossil power generations emit large amounts of the greenhouse gas CO_2 [1,2]. For the energetic utilization of anthropogenic CO_2, dry reforming of methane (DRM, eq. 1) is an interesting option to convert these two greenhouse gases into syngas (CO/H_2 mixtures) [3]. DRM can be integrated in the well-established downstream syngas chemistry leading to synthetic fuels like alcohols or hydrocarbons [4]. Reforming with CO_2, rather than steam reforming with H_2O yields syngas with lower H_2/CO ratios, which is especially attractive for attractive for oxo synthesis (Hydroformylation) of aldehydes from alkenes and possibly also for Fischer–Tropsch synthesis of long-chain hydrocarbons [5,6].

Apart from expensive noble metals, abundant nickel based catalysts are known to be highly active in the dry reforming reaction, but suffer from fast deactivation by coking [7,8] that can even lead to reactor blocking. Carbon deposition originates mainly from the exothermic Boudouard reaction (eq. 2) or from methane decomposition (eq. 3). Additionally, a deviation from the expected $CO:H_2$ ratio of 1:1 composition is usually observed due to the reverse water gas shift reaction (eq. 4). We have recently reported that mitigation of coking over a Ni-based catalyst is possible by operating the reaction at elevated

temperatures of 900 °C [9]. This effect is likely due to the thermodynamic suppression of the Boudouard reaction at such high reaction temperature. Thus, operation at high temperature might be an attractive option for the application of cheap Ni-based catalysts for the DRM reaction.

$$CO_2 + CH_4 \rightarrow 2\ CO + 2\ H_2 \qquad \Delta H_{298} = 247\ kJ\ mol^{-1} \qquad (1)$$

$$2\ CO \rightarrow CO_2 + C \qquad \Delta H_{298} = -172\ kJ\ mol^{-1} \qquad (2)$$

$$CH_4 \rightarrow C + 2\ H_2 \qquad \Delta H_{298} = 75\ kJ\ mol^{-1} \qquad (3)$$

$$CO_2 + H_2 \rightarrow CO + H_2O \qquad \Delta H_{298} = 41\ kJ\ mol^{-1} \qquad (4)$$

While Ni-based catalysts are extensively studied in this reaction [10,11], most reports have looked at reaction temperatures up to around 800 °C. It is thus desirable to learn more about the coking behavior, the structural and catalytic stability at such high temperature where only limited information is available in the literature.

Several attempts have been made to suppress coke formation on Ni catalysts using different supports. The addition of basic promoters such as CaO or MgO to Ni/Al_2O_3 catalysts can increase the activity and reduce carbon formation [12,13]. The Lewis basicity of these promoters enhances the chemisorption of CO_2 [14], a characteristic that is proposed to reduce the Boudouard reaction by shifting the equilibrium towards CO. The relation of carbon deposition and the catalyst structure was studied by Chen and Ren [15] for a Ni/Al_2O_3 catalyst. They reported on the influence of strong $Ni\text{-}Al_2O_3$ interactions on the catalytic properties during DRM. The formation of a $NiAl_2O_4$ spinel was found to have a suppressing effect on the carbon formation. Furthermore, the reduction of $NiAl_2O_4$ compared to NiO results in smaller Ni crystallites [16].

In this work we present an attempt to relate structural stability and redox dynamics of a Ni catalyst with its coking propensity. The catalyst under study contains 55 wt.-% Ni supported on a mixed Mg,Al oxide that was obtained from a co-precipitated Hydrotalcite-like precursor as described in a previous report [9]. The structural and redox stability of the catalyst was tested by subjecting the precursor either to only one calcination and reduction treatment or to multiple TPR/TPO cycles. It has been recently shown that the calcination conditions can have substantial effects on the catalytic performance of $Ni/La_2O_3\text{-}ZrO_2$ catalysts in the low-temperature DRM reaction [17]. On Ni/Al_2O_3 catalysts, Guilhaume et al. [18] have observed significant structural and chemical changes of Ni/Al_2O_3 catalysts as a consequence of such redox cycling. They found, that Ni is initially incorporated in a spinel phase formed with the support and that redox

cycling at low temperatures progressively extracts metallic Ni from the spinel-type structure. While their catalysts were tested in sequential cracking of acetic acid, we have tested our materials for their DRM activity and coke formation rates in a tubular plug-flow reactor and in a magnetic suspension thermobalance.

2 Results and Discussion

2.1 Catalyst preparation and characterization

We have shown recently [9] that Ni nanoparticles supported on a matrix of Mg and Al oxide can be obtained by the preparation of hydrotalcite-like compounds (htl) as well-defined precursor materials. The resulting catalysts are characterized by a homogeneous metal distribution and very small Ni particles that are embedded and therefore stabilized at high temperatures in a Mg,Al mixed oxide matrix. The catalyst used here was prepared via a hydrotalcite-like (htl) precursor of the nominal composition $Ni_{0.5}Mg_{0.17}Al_{0.33}(OH)_2(CO_3)_{0.17} \cdot mH_2O$. The precursor compound can easily be prepared from metal nitrates in a phase-pure form by pH-controlled co-precipitation [9]. The Ni content of 50 mol% (metal based) corresponds to a 55.4 wt.-% Ni loading in the final catalyst. The 1:2 ratio of Mg to Al in the oxidic matrix was chosen to enable $MgAl_2O_4$ spinel formation, a sintering-stable ceramic compound. The platelet-like precursor particles provides a specific BET area of 131 $m^2\ g_{cat}^{-1}$. The calcination was performed at 600 °C. We showed already that this temperature is sufficient for the complete decomposition of the hydrotalcite-like precursor. The calcination in air leads to an increase to 213 $m^2\ g_{cat}^{-1}$ due to shrinkage of the platelets. The characterization details of the phase pure precursor and the calcined product are described in our previous study [9].

The reduction behavior of the calcined material has been investigated using TPR. A single broad peak was observed in the temperature range between 450 and 850 °C. The TPR profile reflects a one-stage process with a maximum at 685 °C (Ni50-TPR1, Figure 1a). On the basis of the TPR profile a reduction temperature of 800 °C was chosen for the following experiments. At this temperature the reduction will be terminated when adding a subsequent holding period of 1 hour. The catalyst obtained after reduction at 800 °C is labeled Ni50-TPR1 in this study. It is characterized by small Ni particles of 11 nm, which are partially embedded in an oxide matrix with a high specific Ni surface area of 25 $m^2\ g_{cat}^{-1}$ (Table 1, Figure

3) [9]. The elemental distribution (Figure 6a), determined by TEM-EDX at different locations is rather homogeneous and the average molar composition is close to the nominal values (Ni/Mg/Al: 57/14/30 (±5); nominal 50/17/33). A comparison of the TPR profile with the reduction profile of a $NiAl_2O_4$ reference material, suggests on a first sight the presence of Ni^{2+} in a $NiAl_2O_4$ phase formed during the first calcination (TPO0). However, the corresponding XRD pattern revealed the presence of a rock salt-type oxide MO (M = Ni, Mg) and a small fraction of Al_2O_3 (Figure 2a). The reflexes in general are relatively broad indicating a low crystallinity. An unambiguous discrimination of NiO and MgO is difficult due to very similar lattice constants and the low crystallinity of the obtained material. Though, the presence of NiO seems more likely looking at higher angles > 100 °2θ, where the differences are more distinct due to the widening of the d-space (see inset Figure 2a). Thus, although the formation of $NiAl_2O_4$ in nickel/alumina catalysts during oxidation is reported in many publications [16,19,20,21,22], our catalyst might be better described as a NiO phase that is strongly interacting with the oxide matrix. Based on XRD, a spinel phase seems to be absent or X-ray amorphous, as no peaks corresponding to $MgAl_2O_4$ or $NiAl_2O_4$ are detectable (Figure 2a). However, the interpretation of the XRD results is usually difficult. Zieliński [16] suggested that the nickel oxide particles are covered by a tight nickel aluminate layer, which determines the reduction behavior while large particles of pure NiO covered by the nickel aluminate layer can be seen in XRD as NiO. This would explain the spinel-like character of the TPR1 profile with simultaneous absence of $NiAl_2O_4$ in the XRD. It has been shown, that higher calcination temperature and longer calcination time increases the metal-support interaction and the fraction of nickel aluminates, resulting in a higher reduction temperature compared to free nickel oxide and increased crystallinity [9,16].

2.2 TPR/TPO cycling

To investigate the influence of redox cycling on the structural properties and on the catalytic performance of the catalyst in detail, consecutive TPR/TPO experiments were conducted. The TPRs were performed up to 800 °C, the TPOs up to 600 °C, analogous to the calcination process. This procedure was repeated several times and the results are presented in Figure 1. The TPR experiments of the calcined or reoxidized Ni50 catalyst are labeled TPR*n*, where *n* is the number of cycles, and the corresponding samples are named Ni50-TPR*n*. Accordingly, the reoxidation profiles are labeled TPO*n*, with *n* as the number of cycles, and the corresponding sample are denoted Ni50-TPO*n*.

During the redox cycles the TPR profile markedly changed (Figure 1a), whereas the total amount of H_2 consumed remained constant and corresponds to a reduction degree of 98% of the NiO. The temperature of maximum hydrogen consumption shifted from 685 °C to 392 °C. Although slight changes might still be present, we consider the system as stable after 16 cycles. Comparison of the profile of TPR16 with the profile of an unsupported NiO reference shows a clear agreement, except for the slowly vanishing shoulder at higher temperatures. We conclude that the (final) Ni phase after 16 reduction-reoxidation cycles consists primarily of NiO. Thus, redox cycling under the applied conditions causes the gradually transition from a strongly interacting "$NiAl_2O_4$–like" into a NiO-like phase with considerably lower interaction to the support. Changes are also observed in the corresponding TPO profiles during reoxidation (Figure 1b). Starting from a single broad peak at 220 °C, the peak maximum is shifted upwards to 313 °C with an arising shoulder at higher temperatures. The still slightly "bimodal" profiles after the cycling (TPR16 and TPO16) suggest the presence of more than one Ni phases, with the above-mentioned NiO being the dominant one. We note that the difference between calcination and TPO is the nature of the catalytic material. A well dispersed hydrotalcite on the one hand and metallic Ni^0 dispersed on the oxide on the other hand. The activity of Ni^0 towards the support oxide is not the same in the two cases. In the second case, the kinetics of the "$NiAl_2O_4$-like" formation is slower. It cannot be excluded that an extended calcination time in the TPO measurements could lead to a spinel-like structure.

After the 20th TPO run, the corresponding XRD pattern revealed an increase in crystallinity of the material in comparison to the primary calcined sample, as suggested by more narrow reflections (TPO20), Figure 2b). The sample can be identified as mainly NiO, which is in agreement with the TPR experiments. The major difference to Ni50-TPO1 is the presence of a spinel phase, which is presumably $MgAl_2O_4$. It is noted that an unambiguous assignment of the spinel phase is not possible by XRD, due to similar lattice constants of $NiAl_2O_4$ and $MgAl_2O_4$ and the still relatively low crystallinity.

The average molar composition of Ni50-TPR21, as determined by TEM-EDX, is still close to the nominal values (Ni/Mg/Al: 52/16/31 (±5); nominal 50/17/33). However, the elemental distribution determined at different locations is not homogeneous anymore. The Ni content is strongly fluctuating (Figure 6b), while the local Mg:Al ratios stays constant at approximately 1:2 in agreement with the formation of $MgAl_2O_4$. This observation indicates that the NiO and the $MgAl_2O_4$ phase segregated as a result of redox cycling as is also suggested by XRD.

TEM and H_2 pulse chemisorption measurements were performed to estimate the dispersion and size of the metallic Ni particles after redox cycling. The structural changes and the thermal stress during cycling result in a significant decrease in Ni surface area and Ni dispersion. The metallic Ni surface area shrinks from 25 for Ni50-TPR1 to 7 $m^2\ g_{cat}^{-1}$ for Ni50-TPR18 (Table 1). This loss of surface area is also reflected in the TEM images where some sintered Ni particles were observed (Figure 4a). However, a statistical evaluation of the particle sizes revealed that the average particle size (arithmetic mean) increased only slightly to 13.4 nm (Table 1) compared to Ni50-TPR1, while the median particle size d_{50} (the diameter where 50% of the measured particles are below/above) even remained constant. However, the size distribution is substantially skewed to larger sizes because of sintering, which is described by the log-normal distribution (Figure 5b). Accordingly, the volume-weighted mean Ni particle size, which is more sensitive to the presence of larger particles, increased to 21.0 nm (Table 1). Ni50-TPR1 on the other hand is characterized by a quite narrow size distribution, as described by the Gauss function (Figure 5a). Hence, the volume-weighted mean Ni particle size is only slightly larger than the arithmetic one in this sample. The presence of crystalline $MgAl_2O_4$ is proven from power spectra evaluation of selected areas of the matrix in TEM images (Figure 4b).In summary, the structural ageing of the Ni50 catalyst upon redox cycling leads to lower dispersion and sintering of the Ni particles produced by reduction. This effect is accompanied by crystallization of the oxide matrix into $MgAl_2O_4$. In the resulting stable Ni/$MgAl_2O_4$ catalyst the interaction of the redox-active Ni phase to the crystalline support is lower than in the starting material as indicated by the lower temperature of the TPR signal. This lower interaction with the crystalline support is likely the origin of a higher particle mobility leading to sintering at high temperature.

Table 1. Composition and particle sizes of the reduced samples determined by TEM and H_2 chemisorption.

Sample label	Particle size distribution[a] / nm			Ni SA[d] / $m^2\ g_{cat}^{-1}$	Ni Dispersion[d] / %
	PS dn[b]	Median d_{50}	PS dv[c]		
Ni50-TPR1	10.4 ± 3.2 (St.D.)	10.4	11.4	25.0	6.8
Ni50-TPR2	-	-	-	20.5	5.6
Ni50-TPR3	-	-	-	14.3	3.9
Ni50-TPR18	-	-	-	7.0	1.9
Ni50-TPR21	13.4 ± 10.1 (St.D.)	10.3	21.0	-	-

[a] determined by TEM
[b] number-weighted mean particle size
[c] volume-weighted mean particle size

[d] measured with H_2 pulse chemisorption

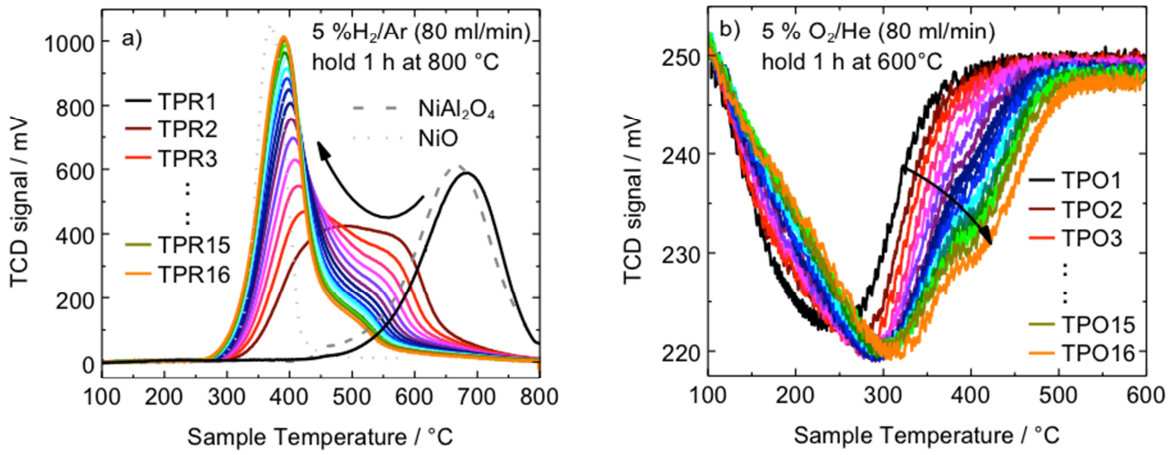

Figure 1. TPR cycles of Ni/MgAl oxide catalyst calcined at 600 °C and of $NiAl_2O_4$ (dark grey dashed line) and NiO (light grey dotted line) as references (a); TPO cycles of Ni/MgAl oxide catalyst (b).

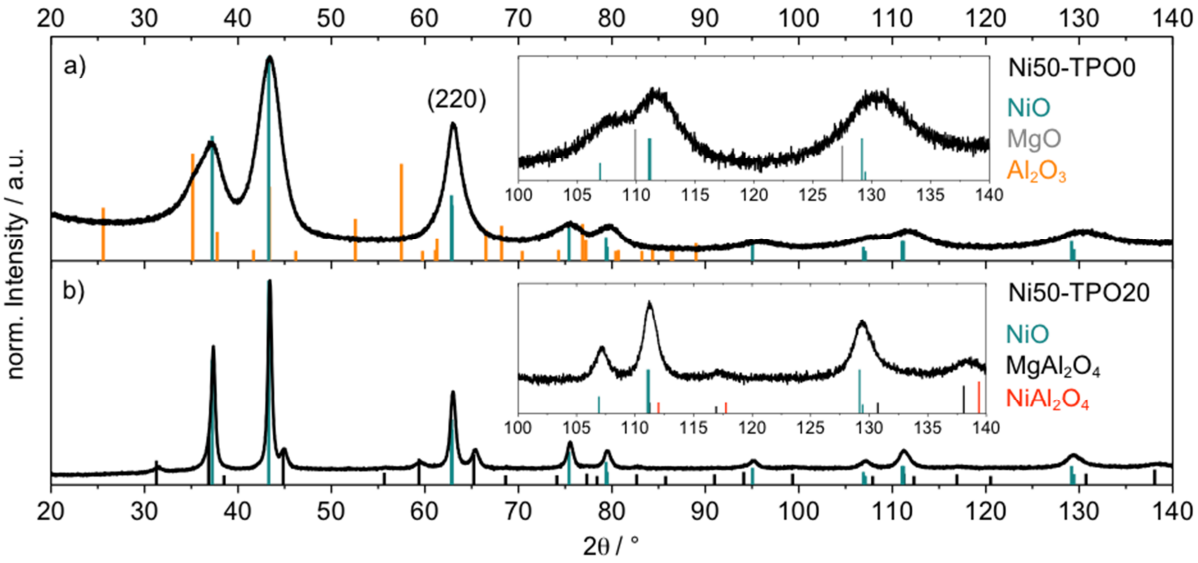

Figure 2. Powder XRD patterns of the mixed oxides after 1. Calcination (TPO0) at 600 °C (a), after TPO20 (b), ICDD 44-1159 NiO (blue), ICDD 89-4248 MgO (grey), ICDD 46-1212 Al_2O_3 (orange), ICDD 21-1152 $MgAl_2O_4$ (black), ICDD 10-0339 $NiAl_2O_4$ (red). Inset figures are magnifications of the range from 100 to 140 °2θ.

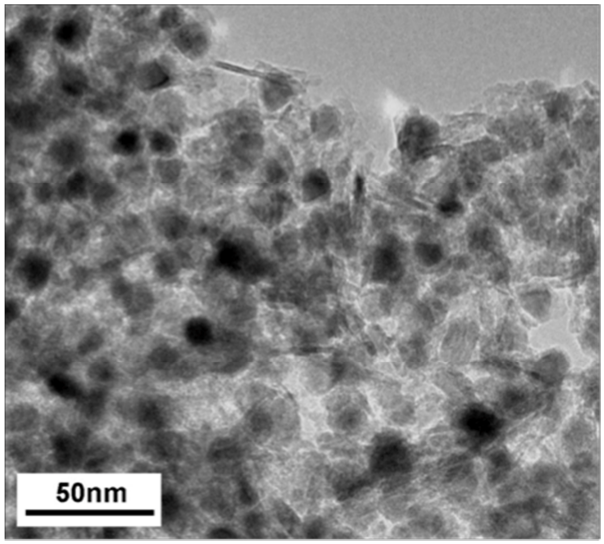

Figure 3. TEM micrographs of reduced Ni50-TPR1 catalyst agglomerate with Ni particles in oxidic matrix.

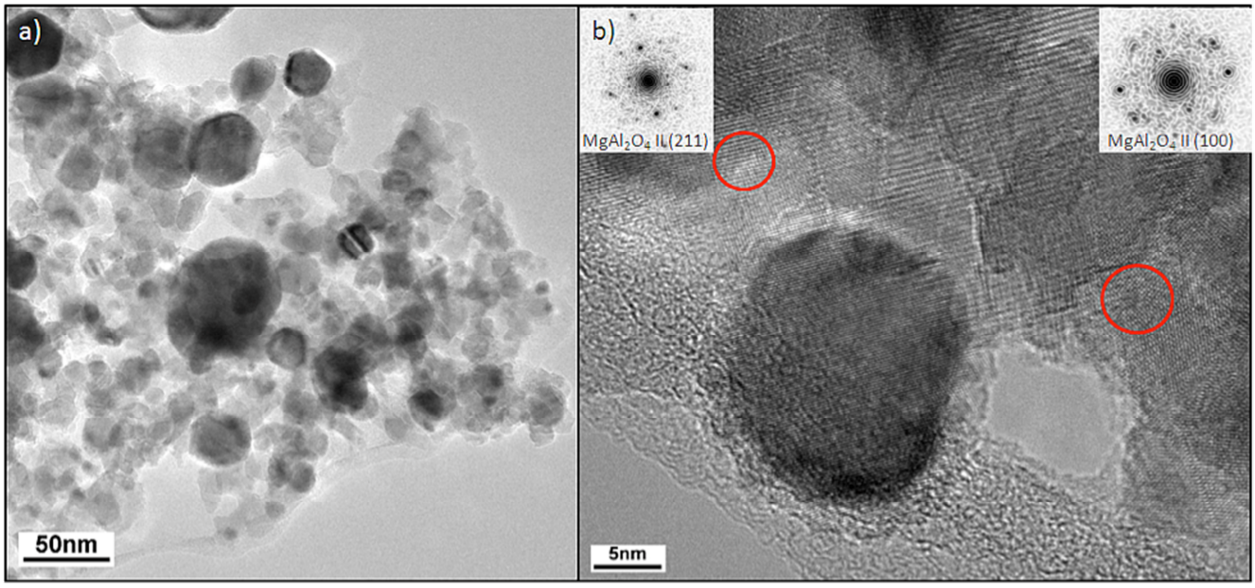

Figure 4. TEM micrographs of 21 times redox cycled sample, Ni50-TPR21; a) catalyst agglomerate with sintered Ni particles, b) Ni nanoparticle in crystalline matrix. Insets are showing the power spectra of selected marked areas of the $MgAl_2O_4$ matrix.

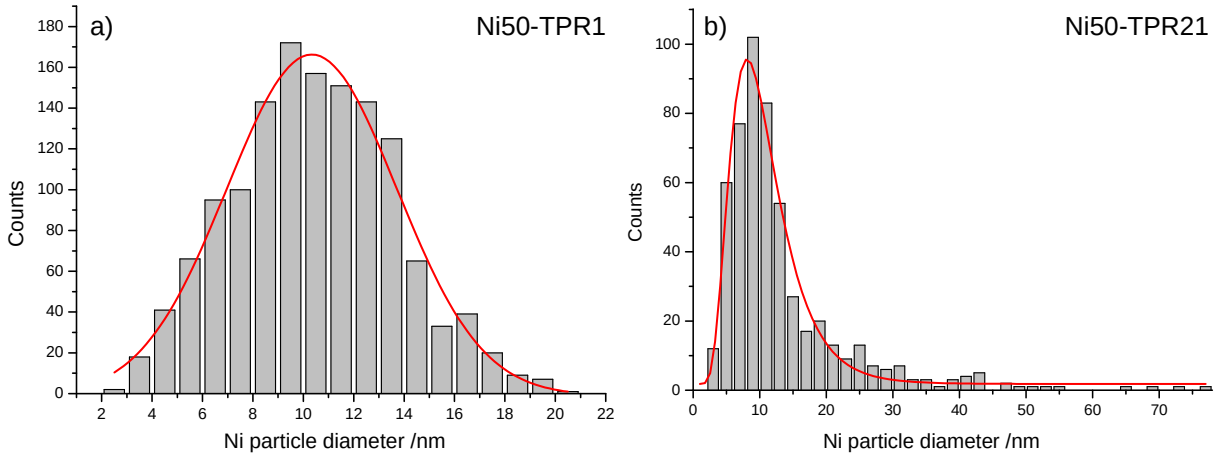

Figure 5. Particle size distributions of Ni50-TPR1 (Gauss distribution) (a) and Ni50-TPR21 (log-normal distribution) (b).

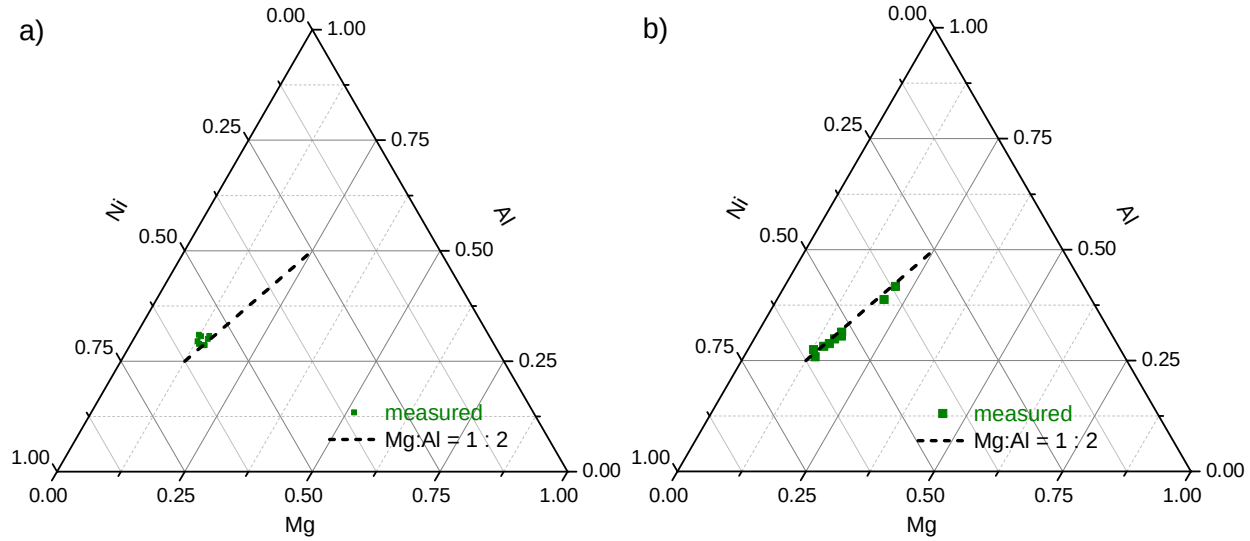

Figure 6. TEM-EDX elemental Ni,Mg,Al distributions of Ni50-TPR1 (a) and Ni50-TPR21 (b).

2.3 Catalytic properties and coking behavior

The effect of the microstructural changes upon redox cycling on the catalytic performance of the fresh catalyst Ni50-TPO0 and of the catalyst Ni50-TPO18 after 18 TPRO cycles was investigated in the dry reforming of methane (DRM) in a tubular reactor. After a reduction up to 800 °C in 4% H_2 in Ar, DRM was performed at an oven temperature of 900 °C for 10 h time on stream with a CO_2/CH_4 feed ratio of 1.25 at atmospheric pressure. The excess of CO_2 is chosen to reduce coke formation. According to Gadalla et al. [5] the temperature limit for carbon deposition increases as the CO_2/CH_4 feed ratio decreases. The degree of methane conversion is given after 1 and after 10 hours. The “fresh” catalyst (equivalent to Ni50-TPR1) performs stably over 10 hours with a high degree of methane conversion of 76 % (Table 2, Figure 7~~Figure~~

~~7~~a). Even in long-term experiments the catalyst showed a remarkable stable activity at 900 °C, still achieving 94 % of the initial CH_4 conversion after 100 h [9]. This is attributed to the stabilizing effect of the oxide matrix. Even though the number of surface metal sites is reduced drastically, the catalytic test of the 19 times TPR/TPO cycled catalyst (equivalent to Ni50-TPR19) resulted in a slightly higher degree of conversion of 79 % with a likewise stable performance over 10 hours (Table 2, Figure 7~~Figure 7~~a). A non-linear relationship of dispersion and catalytic performance has also been reported for other supported Ni catalysts in the DRM reaction [17]. It is noted however that the temperature of the catalyst bed was 735 °C for Ni50-TPR1 and 760 °C for Ni50-TPR19 indicating stronger heat consumption due to the endothermic reaction over the former material. Thus, the observed conversions should not be used for a direct comparison of rates. It is noted that the bed temperatures however were stable during the 10 h experiment indicating stability of the activity for both catalysts.

In summary, the effect of redox cycling leads to a higher effective bed temperature for the sintered catalyst at otherwise similar conversion. Thus, the significant difference in accessible metal sites between the two catalysts is likely reflected in a lower DRM rate leading to a less efficient self-cooling of the catalyst. Both catalysts performed equally stable over 10 hours.

Table 2. Catalytic test results for the Ni/MgAl oxide catalysts for the dry reforming of methane at a furnace temperature of 900 °C and characteristics of spent catalysts.

Sample label	Metal sites[a] / µmol g_{cat}^{-1}	X_{CH_4} (1h) / %	X_{CH_4} (10h) / %	CO_2 formation[b] / mmol g_{cat}^{-1}	C formation[c] / mmol g_{cat}^{-1}
Ni50-TPR1	639	76	76	54	51
Ni50-TPR19	179	79	79	45	98[d]

[a] measured with H_2 pulse chemisorption
[b] measured by TPO after 10 h DRM at T_{oven} = 900 °C in a fixed-bed reactor
[c] measured in a thermobalance after 10h DRM at 900 °C
[d] investigated sample: Ni50-TPR21

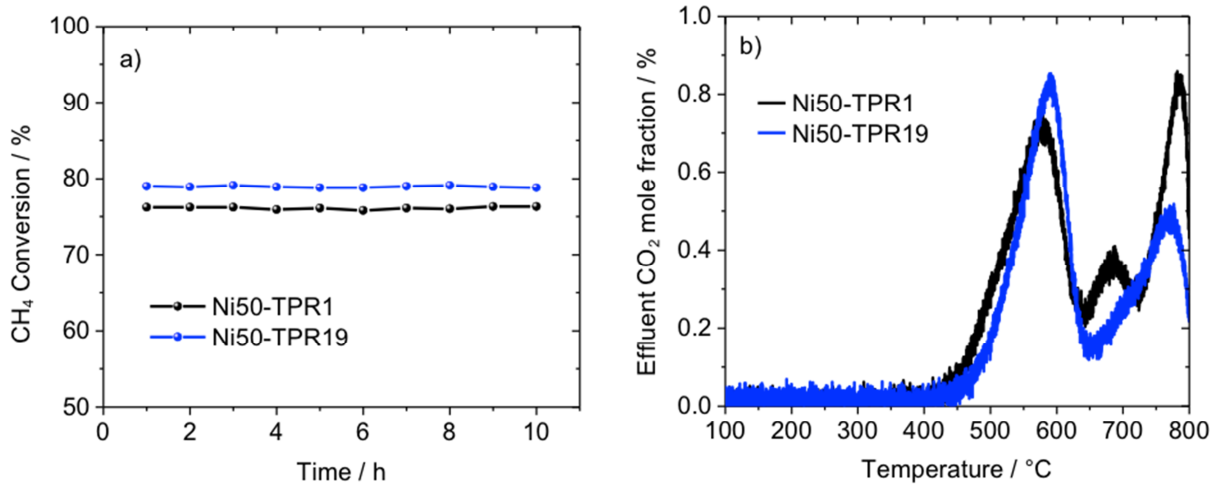

Figure 7. DRM at T_{oven} = 900°C: CH_4 conversion after first reduction and after 18 TPR/TPO cycles (a); TPO profiles of catalysts after 10 h TOS. Effluent mole fractions of CO_2 were detected while heating with 5 K min^{-1} in 4.5% O_2/Ar (b).

The formation of carbon species on the catalysts during DRM was quantitatively and qualitatively detected by different *in situ* characterization methods, such as TPO and thermogravimetry as well as *ex situ* by TEM. In TPO experiments performed subsequent to DRM, the carbon deposits are oxidized to CO_2 in an O_2-containing feed. Partial oxidation to CO was not observed. Therefore, the amount of CO_2 formed is a measure of deposited carbon on the catalyst. The formation of carbonates on the support cannot be excluded. The decomposition of carbonates can interfere with the carbon oxidation. Because the reaction was followed by a holding period of 10 min and cooling in Ar for 2.5 h, carbonates are likely to decompose under these conditions. Therefore the contribution of carbonates is neglected in the following analysis. Despite the similar conversion, the amount of carbon is 54 mmol g_{cat}^{-1} on Ni50-TPR1 and only 45 mmol g_{cat}^{-1} on Ni50-TPR19 (Table 2). This difference might also be affected by the divergent effective bed temperatures. Caused by thermodynamics this can result in a lower amount of carbon at a higher temperature. The corresponding TPO profiles are shown in Figure 7~~Figure 7~~b. On Ni50-TPR1, three distinct peaks are distinguishable at 574, 688 and 781 °C, referring to different carbon species. On Ni50-TPR19, the TPO profile displays the presence of only two distinct carbon species at 591 and 776 °C, the latter showing a pronounced shoulder to lower temperatures.

Düdder et al. [23] performed TPO experiments of carbonaceous reference materials. Referring to their results, we assign the low temperature peak to carbon filaments, whereas the high temperature peak fits

well with the oxidation of high surface area graphite (HSAG). The origin of the small peak in the middle might be assigned to the oxidation of less ordered carbon. Hence, a similar amount of carbon fibers are formed after DRM on both catalysts, but the amount of graphitic carbon, that is thought to originate from methane pyrolysis [9], was significantly reduced by the redox cycling treatment.

The presence of different amounts and types of carbon obtained was also seen in the TEM analysis of the spent catalysts. After DRM of Ni50-TPR1 the initial catalyst morphology is partially still preserved, but the Ni particles are sintered to some extent under working conditions (Figure 8a). In agreement with the TPO results, at least two different carbon species can be found in the TEM micrographs in Figure 8: graphitic carbon layers with and without inclusions of Ni particles (b) and tubular carbon nanofibers (c). Similar results were obtained for the redox cycled catalyst Ni50-TPR19 (Figure 9a), which is also characterized by graphitic as well as filamentous carbon after DRM (Figure 9b,d). In addition to these species, carbon onions with isolated Ni particles were found (Figure 9c). All images indicate significant mobility of a fraction of the Ni particles resulting in detachment from the supporting oxide matrix during formation of carbon fibers ("tip growth"). It is noted that carbon exhibits a significant solubility in Ni at high temperatures [24,25]. Thus, the graphitic onion-like carbon species might have formed by segregation during cooling of a solid Ni-C solution that can form under steady state conditions [26]. The growth mode of carbon on Ni also depends on the particle size. Only small enough particles, which are present in both catalysts, will favor fiber or tube growth, while highly ordered graphene growth and graphite crystallization was observed predominantly on Ni111 terraces [27] that can be expected to a greater extent on larger particles. According to these considerations, a design goal for high-temperature Ni DRM catalysts is the formation of particles that are too large to trigger fiber growth, but at the same time exhibit a low fraction of Ni111 terraces and/or a blocking of carbon dissolution into the bulk by modifications of the surface, e.g. through steps edge blocking [28] or SMSI-layers, or of the bulk, e.g. by the modified sub-surface chemistry of an intermetallic compound [29,30] or alloy [31].

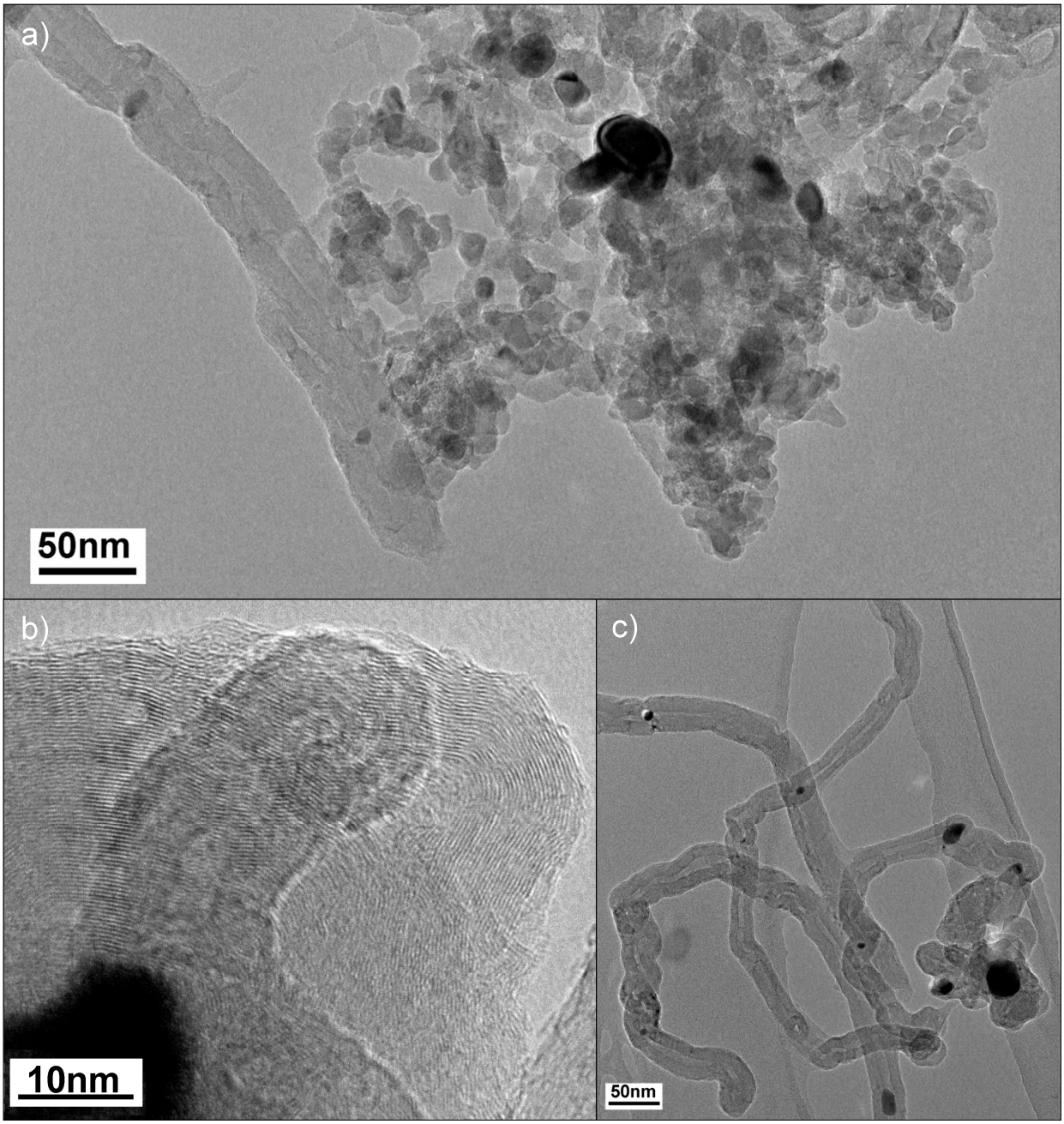

Figure 8. TEM micrographs of the spent Ni50-TPR1, run in DRM for 10 h at a reaction temperature of 900°C: a) catalyst agglomerate, b) Ni particle in graphitic carbon, c) isolated Ni particles in filamentous carbon.

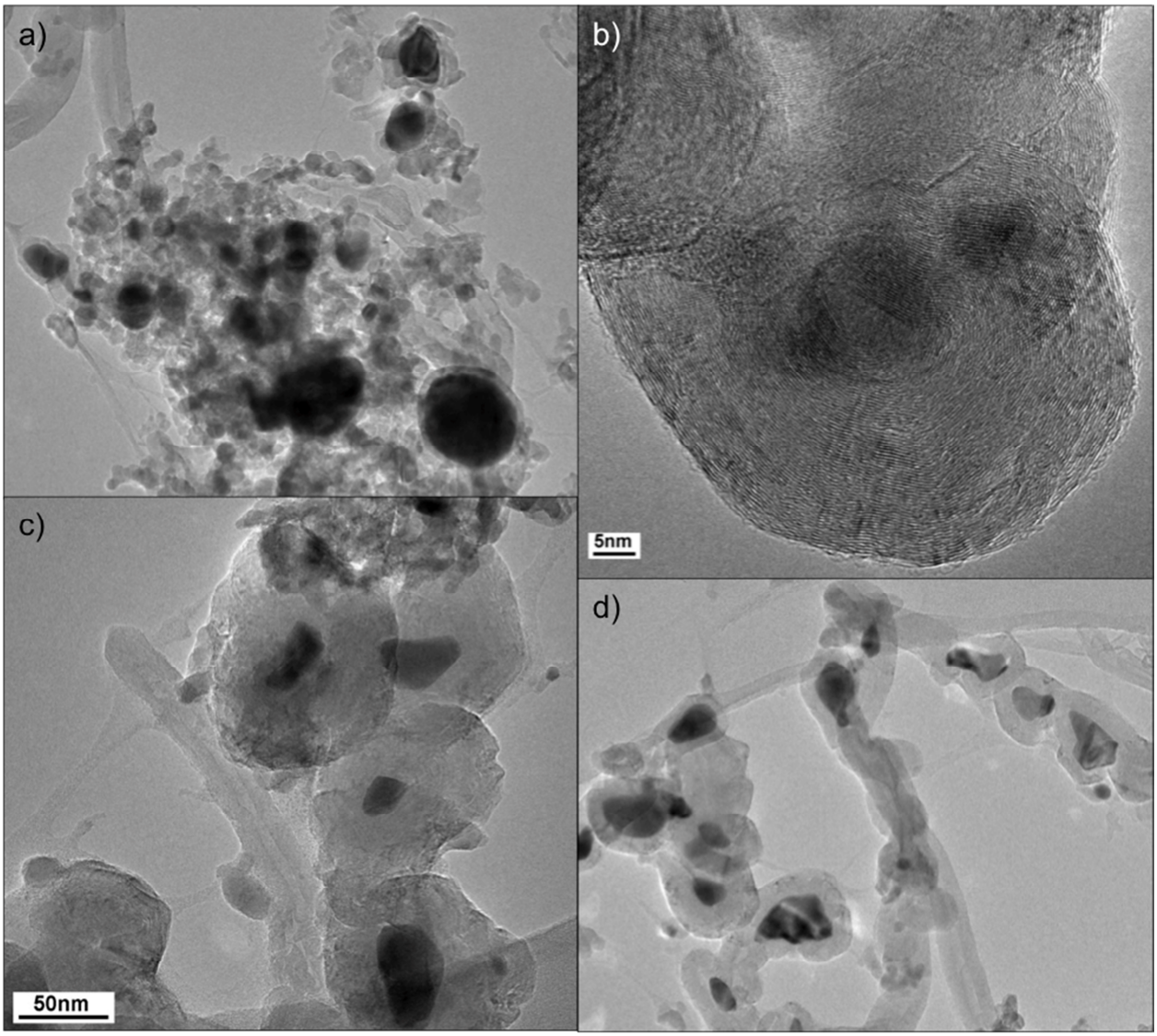

Figure 9. TEM micrographs of the spent Ni50-TPR19, run in DRM for 10 h at a reaction temperature of 900°C: a) catalyst agglomerate, b) Ni particles in graphitic carbon, c) Ni particles in carbon onions, d) Ni particles in filamentous carbon.

Additional to the results obtained in the tubular fixed-bed reactor, the coking kinetics during DRM at $T_{balance}$ = 900 °C of the fresh and of the cycled catalyst have been further explored *in situ* in a thermobalance with a vertical geometry (Figure 10~~Figure 10~~). As in the tubular reactor, the catalysts have been pre-reduced at 800 °C (Figure 10~~Figure 10~~a). The derived mass profiles are in good agreement with the profiles shown during cycling (Figure 1a).

The fresh Ni50-TPR1 was compared to a 21 times cycled Ni50-TPR21 catalyst. In both cases a continuous weight gain was observed during DRM at 900 °C due to carbon formation (Figure 10~~Figure 10~~b). Such an immediate carbon growth without an induction period indicates a rapid saturation of the nickel surface and a prompt nucleation. After 17.5 h a saturation of the carbon formation was found for the

fresh catalyst and after 8 h for the redox cycled one. After leveling carbon is formed with only 0.4 to 0.5 wt.-% h^{-1} and a total amount of about 123 wt.-% carbon was detected for both catalysts. The initial linear formation rate of the carbon deposition was determined to be 7 wt.-% h^{-1} for Ni50-TPR1 and 15 wt.-% h^{-1} for Ni50-TPR21. Thus, the redox cycling resulted in an increased carbon formation rate and an increased total amount of carbon from 51 to 98 mmol g_{cat}^{-1} after 10 h, which is contrary to the observations made in the fixed-bed reactor (Table 2). The decrease in coking rate might be caused by a blocked Ni surface due to carbon depositions and sintering. However, CH_4 conversion (Figure 10~~Figure 10~~c) and the yield of syngas (Figure 10~~Figure 10~~d) were continuously detected in the exhaust gas of the balance by MS. It is noted that a quantitative kinetic evaluation of the MS data is not possible. The large amount of undiluted catalyst, the non-ideal flow conditions and the uncertainties of bed temperature and approach to equilibrium in this experiment do not allow for a reliable catalytic evaluation of activity and stability. Thus, a direct comparability with the experiments in the tubular reactor under much better kinetic control [23] cannot be expected. However, it is noteworthy that the Ni50-TPR21 catalyst seems to be the more active catalyst in the experiment in the thermobalance and shows a higher methane consumption rate. The stability of the catalyst appears to be different in the thermobalance experiment. While both catalysts showed a stable performance over 10 hours in the fixed-bed reactor, in the thermobalance the CH_4 consumption rate increases with time as long as carbon is formed (Figure 10~~Figure 10~~c). Therefore it can be assumed that carbon is mainly formed by methane pyrolysis. This effect is more pronounced for the Ni50-TPR21 catalyst. Carbon saturation is followed by a slow deactivation. However, in the last about 3 hours TOS the conversion seems almost stable (see insets Figure 10~~Figure 10~~c).The H_2 to CO formation ratio (Figure 10~~Figure 10~~d) slowly reaches a value of 1.1 after 20 hours for both catalysts in the expected regime for DRM.

The DRM test was followed by a TPO for regeneration of the catalysts. The corresponding profiles as well as the detected MS signal of CO_2 are displayed in Figure 10~~Figure 10~~e. For both samples, the first weight increase in the TG-TPO profile corresponds to the reoxidation of metallic Ni starting from 250 °C. The subsequent weight decline starting from 450 °C might overlap with the Ni reoxidation and is a result of carbon combustion accompanied by the formation of CO_2. As soon as all CO_2 is evolved the weight increases abruptly around 650 °C. One possible explanation is that next to CO_2, CO is formed during the combustion process. Since CO is a strong reducing agent and can re-reduce the just formed nickel oxide.

After all evolved CO is consumed Ni is oxidized again leading to the abrupt weight increase. An alternative explanation is that two different Ni species are present. One readily accessible Ni species that is not covered with carbon and therefore is oxidized first and another isolated Ni species that is enclosed in graphitic carbon onions, as shown in Figure 9c. To reoxidize this Ni species, the carbon layers have to be removed first. Due to the higher temperatures this 2nd reoxidation happens faster resulting in the abrupt weight increase. Because the mass loss during the reduction is slightly higher than the overall mass gain during the oxidation, the second explanation is more likely. The distinction between different CO_2 peaks is not possible from these measurements in contrast to the TPO experiments subsequent to activity tests in the fixed-bed reactor. This indicates a diffusion limitation due to the high amount of carbon and a lack of oxygen. Carbon on Ni50-TPR1 is oxidized up to higher temperatures. This is in line with the observation of more thermally stable graphitic carbon in the TPO profiles after DRM in the tubular reactor (Figure 7~~Figure 7~~b).In summary, it was shown that the redox dynamics of the hydrotalcite-derived Ni catalyst have a minor effect on the coking behavior in DRM at high temperatures. While the activity may be increased by the redox cycles, the stability is not affected and a lower amount of graphitic carbon deposits was observed after DRM in a fixed-bed reactor. Whereas, complementary performed thermogravimetric DRM measurements identified a carbon limit, independent of the pretreatment. However, the redox cycled catalyst reached this limit more rapidly. Carbon deposits are likely to be formed by methane pyrolysis, which is an undesired side reaction that is promoted by high reaction temperatures, while the exothermic Boudouard reaction shall be thermodynamically hindered. These results show that even at conditions where pyrolysis is favored, there are kinetic factors due to the catalyst's microstructure that can mitigate this side reaction. In the present case, these microstructural effects can be related to the sintering of the Ni particles, their lower interaction to the support and/or the crystalline nature of the $MgAl_2O_4$ spinel. As the change in the TPR profiles and the XRD patterns was much stronger than that in the Ni particle size distribution, we suspect that this effect might rather be related to changes of the oxide component of the DRM catalyst.

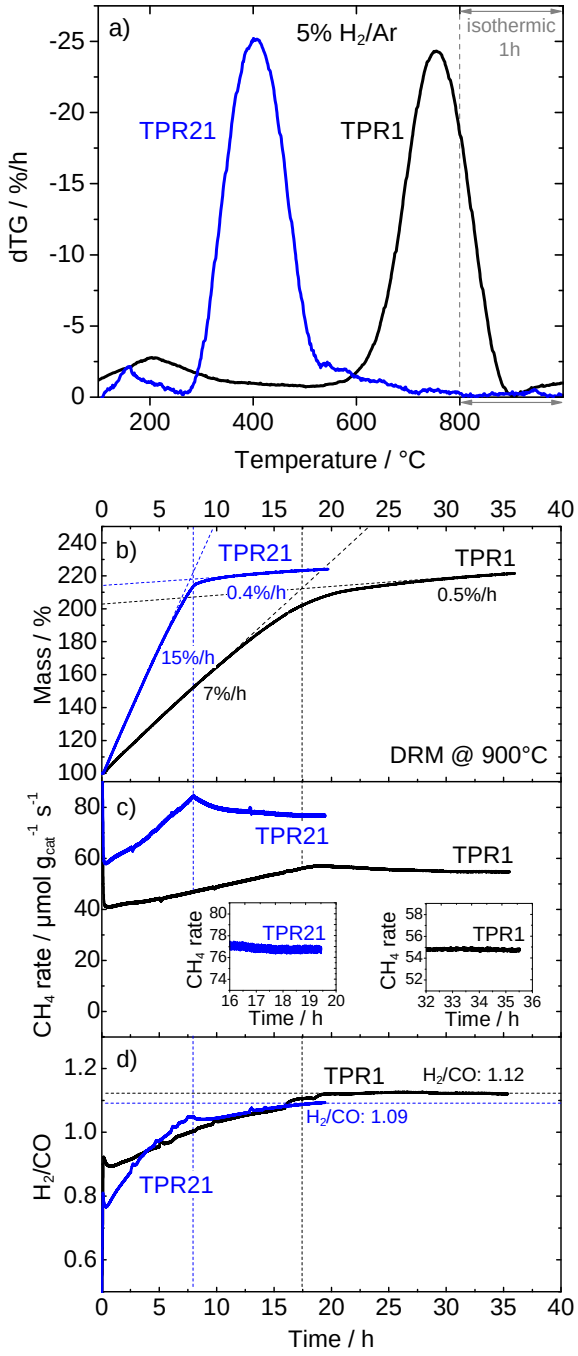
a)
5% H2/Ar
isothermic
1h
TPR21
TPR1
dTG / %/h
Temperature / °C
b)
TPR21
TPR1
0.4%/h
0.5%/h
15%/h
7%/h
DRM @ 900°C
Mass / %
c)
TPR21
TPR1
CH4 rate / µmol gcat-1 s-1
CH4 rate
Time / h
d)
TPR1
H2/CO: 1.12
H2/CO: 1.09
TPR21
H2/CO
Time / h

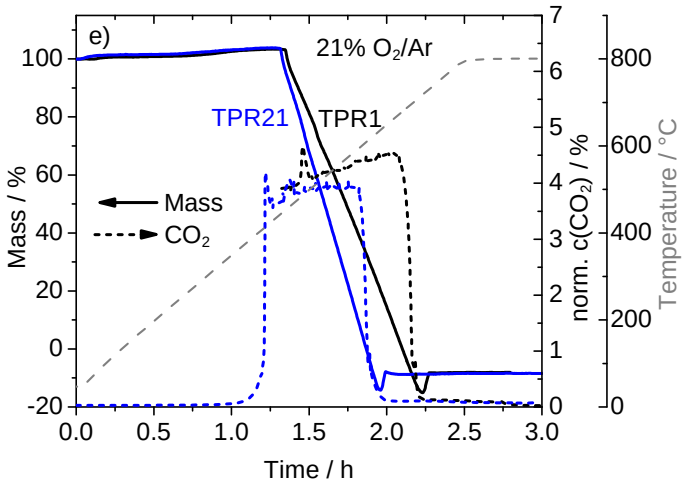

Figure 10. DRM in a thermobalance of Ni50-TPR1 and Ni50-TPR21; pre-reduction in 5% H_2/Ar up to 800 °C (a), DRM at 900 °C (b), CH_4 conversion rate during DRM (c), H_2/CO ratios during DRM (d) and subsequent TPO in 21% O_2/Ar (e).

3 Conclusion

A methodic approach was presented to address the structural stability and the catalytic properties, in particular the coking behavior of Ni-based DRM catalysts at high reaction temperatures. The structural aging of the catalyst was simulated by repeated redox cycles of a hydrotalcite-derived Ni,Mg,Al catalyst. TPR/TPO cycles were found to gradually change the interaction of the redox-active Ni phase with the oxide support resulting in a crystalline Ni/$MgAl_2O_4$-type catalyst. Despite a very high Ni loading of 55.4 wt.-% and high reduction temperature of 800 °C, Ni nanoparticles of a size of only 11 nm were present in the initially prepared catalyst. After cycling the particle size was increased to 21 nm with an increased contribution of larger particles, bringing about a decrease in Ni surface area, while the majority of the particles was still relatively small.

These redox dynamics (TPR/TPO) and the related structural changes were found to have only a moderate influence on the activity in the DRM reaction at 900 °C. However, a decrease in coke deposition was observed after DRM in a fixed-bed reactor, mainly due to a lower fraction of graphitic carbon. Complementary DRM experiments performed in a thermobalance revealed that coke formation is a continuous process until a carbon limit of 123 wt.-% is reached and that the redox cycling leads to faster carbon formation.

Further studies for a deeper understanding of the microstructural changes during redox cycling and their positive effect on coking are needed and planned. The presented analytical methods will be used in the future to study, which structural features of Ni catalysts determine the coking rate in DRM at high temperatures and how they can be tuned by catalyst pre-treatment with the goal to identify an operational window where coking on Ni catalysts can be suppressed to make them functional alternatives to noble-metal based DRM catalysts.

Acknowledgements

We greatly acknowledge the help of Michael Scherzer and Frank Girgsdies for their help with X-ray diffraction measurements and scientific discussions. Financial support was provided by the Federal Ministry of Education and Research of Germany (BMBF, FKZ 01RC1006) within the framework of the “CO2RRECT” project.

4 Material and methods

4.1 Synthesis conditions

The catalyst was prepared from a hydrotalcite-like (htl) precursor with the general formula $Ni_xMg_{0.67-x}Al_{0.33}(OH)_2(CO_3)_{0.17} \cdot mH_2O$ (x= 0.5) by constant pH *co-precipitation*. The amount of nickel was 50 mol%, and equates to a Ni-loading of 55.4 wt% in the final catalyst. The precipitation took place in an automated laboratory reactor (Mettler-Toledo Labmax) at T=50 °C from aqueous 0.6 M NaOH, 0.09 M Na_2CO_3 solution and 0.4 M aqueous metal nitrate solution at pH 8.5. The precipitate was aged for 0.5 h in the mother liquor at 50 °C, filtrated, thoroughly washed with water until the conductivity of the filtrate was < 0.5 mS cm^{-1} and dried at 100 °C over night. The obtained precursor was calcined in air at 600 °C for 3 h.

4.2 Characterization

Powder X-ray diffraction (XRD) measurements were performed using a Bruker D8 Advance reflection diffractometer equipped with a Lynx-Eye energy discriminating position sensitive detector (1D-PSD) using CuK radiation. Kβ radiation was suppressed with a Ni-filter. Step scans were performed from 5 to 140° 2θ and a step size of 0.02° with a count time of 1 s/step.

Specific surface areas of the calcined material and the precursors were carried out by N_2 physisorption (Quantachrome Autosorb-6) and evaluated using the BET method. The samples were outgassed for 4 h at 80°C.

Temperature-programmed reductions (TPR) of the sample (41 mg) were performed in a fixed-bed reactor (TPDRO-1100, CE Instruments). Prior to the TPR measurements, the sample was pretreated at 300 °C for 30 min in 5 % O_2/He to remove moisture and other adsorbed impurities. The TPR measurements were performed up to 800 ° in 5 % H_2/Ar (80 Nml min^{-1}), with a heating rate of 6 K min^{-1}, in a quartz tube. The final temperature was hold for 1 h. The H_2 consumption was monitored with a thermal conductivity detector (TCD). The TCD detector was calibrated by reducing a known amount of CuO. Likewise, the *temperature-programmed oxidations (TPO)* were performed up to 600 °C in 5 % O_2/He (80 Nml min^{-1}), with a heating rate of 6 K min^{-1}, in a quartz tube. The final temperature was hold for 1 h.

To determine the *nickel metal surface area*, a H_2 pulse chemisorption method was applied. Therefore the samples were reduced in 5% H_2/Ar (80 Nml min^{-1}), with a heating rate of 6 K min^{-1} in a fixed-bed reactor. After cooling down to 50 °C in Ar, a defined volume of H_2 gas (100 %) is introduced by pulse-dosing with a

volume of 250 µl. The pulses were continued until no further uptake was detected. The Ni metal surface area was determined assuming a dissociative chemisorption mechanism of hydrogen (Sf= 2; $2Ni/H_2$) [32].

The microstructure of the samples was examined by using Philips CM200 *transmission electron microscopes (TEM)* equipped with a LaB_6 cathode or a field electron gun. High-resolution images were taken with a CCD camera. For good statistics 40 to 80 images were taken for each sample on different agglomerates and regions of the catalysts. For the investigation of the microstructure of the activated catalysts the samples were reduced and subsequent passivated by slow increase of oxygen partial pressure at room temperature. For the investigation of catalysts after DRM the samples were reactivated by reduction and exposed to a second DRM run with the conditions described above to obtain the spent samples for microstructural characterization. After cooling down, the catalysts were separated from the dilutant by sieving. All samples were dispersed in chloroform and deposited on a holey carbon film supported on a copper grid.

Thermogravimetric experiments for the investigation of coking behavior have been performed in a Rubotherm thermobalance. Prior the experiment 120 mg (Ni50-TPR1) or 80 mg (Ni50-TPR21) of the catalyst was reduced with 5 K min^{-1} at 800 °C in 5% H_2/Ar. Upon reaching the desired reaction temperature the system was purged in Ar for 1 h. Afterwards the DRM was performed at 900 °C in 120 Nml min^{-1} 40% CO_2 / 32% CH_4 / Ar for 10h. Subsequent to the reaction the carbonaceous deposits were oxidized in 21% O_2/Ar (214 Nml min^{-1}) and a linear heating rate of 5 °C min^{-1}. The final temperature of 800 °C was held for 1 h.

4.3 Catalytic performance

The *catalytic experiments* were performed in a continuous flow system at atmospheric pressure using a fixed-bed tubular quartz reactor of 8 mm inner diameter. For steady state measurements a calibrated on-line GC (Shimadzu 14-B) was used to analyze the product gas composition. For transient studies a coupled IR-detector (CO, CO_2 & CH_4) and a TCD for H_2 (Emerson MLT4 multi channel analyzer) and a paramagnetic O_2 detector (Magnos 16) were used.

For the catalytic test, 10 mg of the calcined catalyst (sieve fraction of 250-355 µm) was diluted with 490 mg of high purity SiC (sieve fraction of 125-180 µm). Initially, the catalyst was activated by reduction in 4% H_2/Ar (99,9 %/99,999 %) and a total flow of 20 Nml min^{-1} with a linear heating rate of 5 °C min^{-1}. The final temperature was held constant for 30 min. Afterwards the catalyst was heated to the reaction temperature

of 900 °C in Ar (99,999 %). The dry reforming reaction was carried out with a gas mixture consisting of CH_4 (99,9995 %), CO_2 (99,9995 %) and Ar in a ratio of 32:40:28. The total flow was set to 240 Nml min^{-1}. The reaction was performed at constant furnace temperature with a reaction time of 10 h. The reaction was followed by a holding period of 10 min and cooling in Ar for 2.5 h. In case the sample was not ex-situ characterized by TEM directly after DRM, a subsequent TPO experiment was performed with a flow rate of 40 Nml min^{-1} of 4.5% O_2/Ar (99,995 %/99,999 %) and a linear heating rate of 5 °C min^{-1}. The final temperature of 800 °C was held constant until no more O_2 consumption was observed.

5 Literature

[1] M. Steinberg, *Int. J. Hydrogen Energ.* **1999**, 24, 771-777.

[2] D. A. Lashof, D. R. Ahuja, *Nature* **1990**, 5, 344, 529-531.

[3] R. Navarro, B. Pawelec, M.C. Alvarez-Galván, R. Guil-Lopez, S. Al-Sayari, J.L.G. Fierro, *Green Ener. Technol.* **2013**, 137, 45-66.

[4] T. V. Choudhary, V. R. Choudhary, *Angew. Chem. Int. Ed*. **2008**, 47, 1828-1847.

[5] A. M. Gadalla, B. Bower, *Chem. Eng. Sci.* **1988**, 43, 3049-3062.

[6] Y. Lu, T. Lee, *J. Nat. Gas Chem.* **2007**, 16, 329-341.

[7] A. T. Ashcroft, A. K. Cheetham, M. L. H. Green, P. D. F. Vernon, *Nature* **1991**, 352, 225-226.

[8] S. Wang, G. Q. Lu, *Energy & Fuels* **1996**, 10, 896-904.

[9] K. Mette, S. Kühl, H. Düdder, K. Kähler, A. Tarasov, M. Muhler, M. Behrens, *ChemCatChem* **2014**, 6, 100-104.

[10] M. C. J. Bradford, M. A. Vannice, *Catal. Rev.: Sci. Eng.* **1999**, 41, 1-42.

[11] M.-S. Fan, A. Z. Abdullah, S. Bhatia, *ChemCatChem* **2009**, 1, 192-208.

[12] Z. L. Zhang, X. E. Verykios, Catal. *Today* **1994**, 21, 589-595.

[13] S.-B. Tang, F.-L. Qiu, S.-J. Lu, *Catal. Today* **1995**, 24, 253-255.

[14] G. J. Kim, D.-S. Cho, K.-H. Kim, J.-H. Kim, *Catal. Lett.* **1994**, 28, 41-52.

[15] Y.-G. Chen, J. Ren, *Catal. Lett.* **1994**, 29, 39-48.

[16] J. Zieliński, *J. Catal*. **1982**, 76, 157-163.

[17] S. Sokolov, E.V. Kondratenko, M.-M. Pohl, U. Rodemerck, *Inter. J. Hydr Ener.* **2013**, 38, 16121-16132.

[18] T. Davidian, N. Guilhaume, H. Provendier, C. Mirodatos, *Appl. Catal. A.* **2008**, 337, 111-120.

[19] C. H. Bartholomew, R. J. Farrauto, *J. Catal.* **1976**, 45, 41-53.

[20] P. Salagre, J. L. G. Fierro, F. Medina, J. E. Sueiras, *J. Mol. Catal. A: Chem*. **1996**, 106, 125-134.

[21] J. M. Rynkowski, T. Paryjczak, M. Lenik, *Appl. Catal., A* **1993**, 106, 73-82.

[22] C. Li, Y.-W. Chen, *Thermochim. Acta* **1995**, 256, 457-465.

[23] H. Düdder, K. Kähler, B. Krause, K. Mette, S. Kühl, M. Behrens, V. Scherer, M. Muhler, submitted to *Catal. Sci. Technol.* **2014**.

[24] R.S. Weatherup, B. Dlubak, S. Hofmann *ACS Nano* **2012**, 6, 9996–10003.

[25] A. Rinaldi, J. P. Tessonnier, M. E. Schuster, R. Blume, F. Girgsdies, Q. Zhang, et al. *Angew. Chem. Inter. Edit.* **2011**, 50, 3313-3317.

[26] R. S. Weatherup, B. C. Bayer, R. Blume, C. Baehtz, P. R. Kidambi, M. Fouquet, et al. *ChemPhysChem*, **2012**, 13, 2544-2549.

[27] L. L. Patera, C. Africh, R. S. Weatherup, R. Blume, S. Bhardwaj, C. Castellarin-Cudia, A. Knop-Gericke, R. Schlögl, G. Comelli, S. Hofmann, C. Cepek, *ACS Nano* **2013**, 7, 7901-7912.

[28] F. Abild-Pedersen, J. Greeley, J. K. Nørskov, *Catalysis Letters* **2005**, 105, 9-13.

[29] S. Saadi, B. Hinnemann, S. Helveg, C. C. Appel, F. Abild-Pedersen, J. K. Nørskov. *Surface Science* **2009**, 603, 762-770.

[30] M. Armbrüster, M. Behrens, F. Cinquini, K. Föttinger, Y. Grin, A. Haghofer, B. Klötzer, A. Knop-Gericke, H. Lorenz, A. Ota, S. Penner, J. Prinz, C. Rameshan, Z. Révay, D. Rosenthal, G. Rupprechter, P. Sautet, R. Schlögl, L. Shao, L. Szentmiklósi, D. Teschner, D. Torres, R. Wagner, R. Widmer, G. Wowsnick, *ChemCatChem* **2012**, 4, 1048-1063.

[31] B. Steinhauer, M.R. Kasireddy, J. Radnik, A. Martin, *Appl. Catal. A* **2009**, 366, 333-341.

[32] M. Fadoni, L. Lucarelli, *Stud. Surf. Sci. Catal.* **1999**, 123, 289-342.